China Geology 1 (2021) 111−125

China Geology

Journal homepage: http://chinageology.cgs.cn
https://www.sciencedirect.com/journal/china-geology

Petrology and metamorphism of glaucophane eclogites in Changning-Menglian suture zone, Bangbing area, southeast Tibetan Plateau: An evidence for Paleo-Tethyan subduction

Yu-zhen Fu[a, b], Zhi-ming Peng[c,*], Bao-di Wang[c], Guo-zhi Wang[a, b], Jing-feng Hu[d], Jun-lei Guan[c], Ji Zhang[d], Zhang Zhang[c], Yun-he Liu[d], Zou Hao[a, b]

[a] *College of Earth Sciences*, *Chengdu University of Technology*, *Chengdu* 610059, *China*
[b] *Key Laboratory of Tectonic Controls on Mineralization and Hydrocarbon Accumulation of Ministry of Natural Resources*, *Chengdu University of Technology*, *Chengdu* 610059, *China*
[c] *Chengdu Center of China Geological Survey*, *Ministry of Natural Resources*, *Chengdu* 610081, *China*
[d] *Institute No.*280 *of China National Nuclear Corporation*, *Guanghan* 618300, *China*

ARTICLE INFO

Article history:
Received 30 September 2020
Received in revised form 1 February 2021
Accepted 22 February 2021
Available online 5 March 2021

Keywords:
Eclogite
HP/UHP metamorphism
Subduction channel
Changning-Menglian suture zone
Paleo-Tethyan subduction
Geological survey engineering
Southeast Tibetan Plateau

ABSTRACT

High/ultrahigh-pressure (HP/UHP) metamorphic complexes, such as eclogite and blueschist, are generally regarded as significant signature of paleo-subduction zones and paleo-suture zones. Glaucophane eclogites have been recently identified within the Lancang Group characterized by accretionary mélange in the Changning-Menglian suture zone, at Bangbing in the Shuangjiang area of southeastern Tibetan Plateau. The authors report the result of petrological, mineralogical and metamorphism investigations of these rocks, and discuss their tectonic implications. The eclogites are located within the Suyi blueschist belt and occur as tectonic lenses in coarse-grained garnet muscovite schists. The major mineral assemblage of the eclogites includes garnet, omphacite, glaucophane, phengite, clinozoisite and rutile. Eclogitic garnet contains numerous inclusions, such as omphacite, glaucophane, rutile, and quartz with radial cracks around. Glaucophane and clinozoisite in the matrix have apparent optical and compositional zonation. Four stages of metamorphic evolution can be determined: The prograde blueschist facies (M_1), the peak eclogite facies (M_2), the decompression blueschist facies (M_3) and retrograde greenschist facies (M_4). Using the Grt-Omp-Phn geothermobarometer, a peak eclogite facies metamorphic *P-T* condition of 3000–3270 MPa and 617–658°C was determined, which is typical of low-temperature ultrahigh-pressure metamorphism. The comparison of the geological characteristics of the Bangbing glaucophane eclogites and the Mengku lawsonite-bearing retrograde eclogites indicates that two suites of eclogites may have formed from significantly different depths or localities to create the tectonic mélange in a subduction channel during subduction of the Triassic Changning-Menglian Ocean. The discovery of the Bangbing glaucophane eclogites may represent a new oceanic HP/UHP metamorphic belt in the Changning-Menglian suture zone.

1. Introduction

High-pressure to ultrahigh-pressure (HP/UHP) metamorphic complexes of blueschist to eclogite facies are significant signature of paleo-subduction zones and paleo-suture zones among plates. They recorded the tectonic evolution processes of subduction and exhumation of the crustal (both oceanic and continental) materials. Therefore, discovering and investigating HP/UHP metamorphic complexes is the key process to identify (ultra-) high pressure metamorphism and to understand the deep subduction process of the lithosphere (Maruyama S et al., 1996; Ernst WG, 2006; Zhang LF, 2008; Wei CJ and Clarke GL, 2011). The Tibetan Plateau and its southeastern margin belong to the eastern part of the Tethyan tectonic regime, and during the subduction and collision between the Paleo-Tethys oceans and continents, characteristic HP/UHP metamorphic rocks commonly formed. The Changning-Menglian suture zone at the southeastern margin and the Longmucuo-Shuanghu suture zone at the northern part of the Tibetan Plateau are important components

First author: *E-mail address*: fuyuzhen15@cdut.edu.cn (Yu-zhen Fu).
* Corresponding author: *E-mail address*: pzm20022002@163.com (Zhi-ming Peng).

doi:10.31035/cg2021017
2096-5192/© 2021 China Geology Editorial Office.

of the eastern aleo-Tethys Ocean. Similar lithological assemblages, typical of a subduction-accretionary setting containing ophiolitic mélanges (Jian P et al., 2009; Wang BD et al., 2013), shallow marine carbonates, deep-sea deposits (Peng T et al., 2008; Sone M and Metcalfe I, 2008; Jian P et al., 2009; Metcalfe I, 2011), arc volcanics (Peng T et al., 2008) and HP/UHP metamorphic complexes (Zhang RY et al., 1993; Fan WM et al., 2015; Li J et al., 2015; Wang F et al., 2016) developed in these two zones. Hence, the Longmucuo-Shuanghu suture zone and Changning-Menglian suture zone likely represent a united residual of the Paleozoic Tethys Ocean. The location is where the main ocean basin of the paleo-Tethys Ocean has developed, probably from Cambrian to Permian (Li C et al., 2008, 2010; Wang BD et al., 2013, 2018; Wang DB et al., 2016; Sun ZB et al., 2017; Liu GC et al., 2017; Peng ZM et al., 2014a, 2014b, 2018b). For the Longmucuo-Shuanghu suture zone at the northern Tibetan Plateau, a high-pressure metamorphic rock suite of Triassic blueschists and oceanic eclogites has already been identified (Bao P et al., 1999; Dong YS and Li C, 2009; Li C et al., 2009; Liang X et al., 2017; Liu Y et al., 2011; Zhai QG et al., 2011a, 2011b). Whereas for the Changning-Menglian suture zone at the southeastern Tibetan Plateau, reports on eclogites are rare although Triassic blueschists has been discovered. Peng XJ (1982) for the first time discovered blueschists in the metamorphic rocks of the Lancang Group and the subsequent studies on the blueschists are mainly about the spatial distribution (Zhang RY et al., 1990; Zhao J, 1993; Zhang ZB et al., 2004; Fan WM et al., 2015; Wang F et al., 2016; Sun ZB et al., 2020; Wang HN et al., 2020a), geochronology (Zhang RY et al., 1990; Zhao J et al., 1993, 1994; Fan WM et al., 2015), geochemistry (Fan WM et al., 2015; Wang F et al., 2016; Wang HN et al., 2020a), and the formation temperature-pressure condition (Zhang RY et al., 1990; Zhai MG et al., 1990; Zhao J et al., 1994; Fan WM et al., 2015; Sun ZB et al., 2020). The results showed that blueschists in that region formed at similar age in Triassic as the blueschists in the Longmuchuo-Shuanghu suture zone. The metamorphic ages are 214 Ma, 238 Ma, and 242 Ma (Zhang RY et al., 1990; Zhao J, 1993; Fan WM et al., 2015). Recently, Li J et al. (2015, 2017) for the first time discovered garnet amphibolite in the Wanhe ophiolitic complex located between the Lincang arc granites and the Lancang Group. They interpreted the formation of the garnet amphibolite as from retrograde metamorphism of eclogites with the peak metamorphism at P=3.35–4.46 GPa, T=530–610°C. Wang HN et al. (2019) further showed that the garnet amphibolite should be lawsonite-bearing retrograded eclogites with the peak metamorphic P-T conditions of 2.4–2.6 GPa and 520–530°C, peak metamorphic ages of 246 ± 2 Ma and 245 ± 2 Ma, and protolith age of 451 ± 3 Ma. And then the discovery of eclogite was reported in the Wanhe ophiolitic mélange (Sun ZB et al., 2019).

Since 2017, the group for the first time discovered fresh glaucophane eclogites in the blueschist belt of the Lancang Group during our 1∶50000 regional geological survey on the Changning-Menglian suture zone (Peng ZM et al., 2018a, 2019). This discovery provides important clues to further understand the tectonic evolution of the Tethyan regime. This article focuses on glaucophane eclogite and studies the occurrence characteristics of the eclogites, and the formation and evolutionary processes, to shed light on the deep subduction and exhumation processes of the paleo-Tethys Ocean.

2. Geological setting

The Changning-Menglian suture zone at the southeastern Tibetan Plateau is located between the Baoshan block to the west and the Lincang-Menghai magmatic arc to the east. The zone is connected to the Longmucuo-Shuanghu suture zone to the north and the Qingmai suture zone in Thailand and the Bentong-Raub suture zone in Malaysia to the south (Fig.1a). Widespread ophiolitic complexes, lithological assemblages representing residual oceanic islands and seamounts, and blueschists in the region are signatures for the subduction and collision of the Paleo-Tethys Ocean (Wang BD et al., 2018), in which the blueschists mainly occur in the Lancang Group.

The Lancang Group is located between the Changning-Menglian ophiolitic complex belt and the Lincang arc granitic belt (Fig. 1b) and distributes along an elongated belt from the Fengqing County in the north, via the Yun County, Lincang, Shuangjiang, and Lancang counties, to the Xishuangbanna Prefecture in the south. According to the latest 1∶50000 regional geological survey (Peng ZM et al., 2018a), the metamorphic complex is mainly composed of the Lancang Group. The group is dominated by schist, including meta-basic rocks, meta-acid rocks and high-pressure metamorphic rocks which discretely occur as blocks and lenses. The schist includes metasedimentary rocks and meta-volcanic rocks. The metasedimentary rocks are represented mainly by mica-quartz schist and biotite-muscovite schist. The meta-volcanic rocks are made up of greenschist, albite schist and amphibole schist. Geochronological studies showed that zircon U-Pb ages of the meta-volcanic rocks of the Lancang Group concentrate at 462–454 Ma (Nie XM et al., 2015; Xing X et al., 2017) and the youngest peaks of detrital zircon U-Pb ages of the metasedimentary rocksoccur at 530–560 Ma and 450–428 Ma (Wang F et al., 2017; Wang BD et al., 2018; Wang HN et al., 2020a).

The Lancang Group has experienced three stages of metamorphic deformation (Peng ZM et al., 2018a). The first stage of deformation occurred during decease of the subduction of the Paleo-Tethys Ocean. Regional near north-south trending foliation S_n and syn-deformation regional metamorphism at blueschist facies were generated due to ductile shearing deformation. The second stage of deformation happened during the collision between the Baoshan and the Simao blocks, during which mylonitic foliation S_{n+1}, locally overprinting S_n, and syn-deformation dynamic metamorphism at greenschist facies were formed by strike-slip shearing deformation. The third stage of deformation took place during the continuous collision between the Baoshan and Simao blocks. Earlier foliations were folded and deformed, and S_{n+2} was formed locally. A series of thrust faults were generated due to thrusting and

detachment, leading to post-deformation retrograde metamorphism of the greenschist facies. Overall, the tectonic pattern of the Lancang Group is exhibited as thrust-nappe accretionary mélange created during the eastward Early Paleozoic subduction of the Changning-Menglian Ocean.

3. Field geological characteristics of the eclogite

Two blueschist belts have developed in the Lancang Group characterized by accretionary mélange (Zhang ZB et al., 2004; Wang HN et al., 2020a). They are the Suyi blueschist belt and the Nanlang blueschist belt. Glaucophane eclogites mainly appear in the Bangbingxiang area of the Suyi blueschist belt (Fig. 1b). Exposure of the eclogites outcrops is about 500 m wide and distributes in a near north-south direction for a few hundred meters. The eclogites newly found in this paper occur in coarse-grained garnet-mica schist with intensive deformation. The eclogites feature different scales ranging from more than 50 m thick to about 1–2 m thick. The eclogites are produced in the form of lenses, which is a typical feature of accretionary complexes (block-in-matrix) (Figs. 2a–b). The eclogites feature weak retrograde metamorphism. Therefore, they are pretty fresh and well preserved (Figs. 2c–d).

4. Analytical techniques

Mineral analyses were performed using a JEOL JXA-8230 electron probe microanalyzer with four wavelength-dispersive spectrometers (WDS) at the Center for Global Tectonics, School of Earth Sciences, China University of Geosciences (Wuhan). The operating conditions were described in Wang J et al. (2019) and Ning WB et al., (2019) in detail. 15 kV accelerating voltage, 20 nA probe current, and 1 or 5 micron beam diameter had been used based on different minerals. Dwell times were 10 s on element peaks and half that on background locations adjacent to peaks. A series of natural and synthetic SPI standards were utilized and changed based on the analyzing minerals. Standards used in this study were: Orthoclase for K; diopside for Ca; magnetite for Fe; jadeite for Na; pyrope for Mg; Y-Al garnet for Al; albite for Si; rutile for Ti; rhodonite for Mn. Raw X-ray intensities were corrected using a ZAF (atomic number, absorption, fluorescence) correction procedure. All element concentraions accurately reproduced standard compositions within about 2%, most elements within about 1% of relative error. Geochemical compositions of representative minerals in the eclogites are listed in Table 1 and Table 2 and the sampling location is shown in Fig. 1b.

5. Petrography and mineral chemistry of the eclogite

According to the mineral assemblages, two types of rocks including glaucophane eclogite and actinolite-bearing eclogite have been identified in the same lenses of eclogites. As the main research object in this paper, glaucophane eclogites are present in grayish-green with porphyroblastic texture and blocky structure (Figs. 2c–d). It can be observed that the porphyroblasts are mainly garnet (20%–30%) and glaucophane (10%), and occasionally clinozoisite (5%–10%). The metamorphosed matrix with granular crystalloblastic texture, mainly consists omphacite (40%–50%), glaucophane (5%), chlorite (5%), quartz (5%) and minor amount of phengite (<3%), and rutile (3%). In most eclogites, garnet, omphacite, and glaucophane are homogeneously distributed.

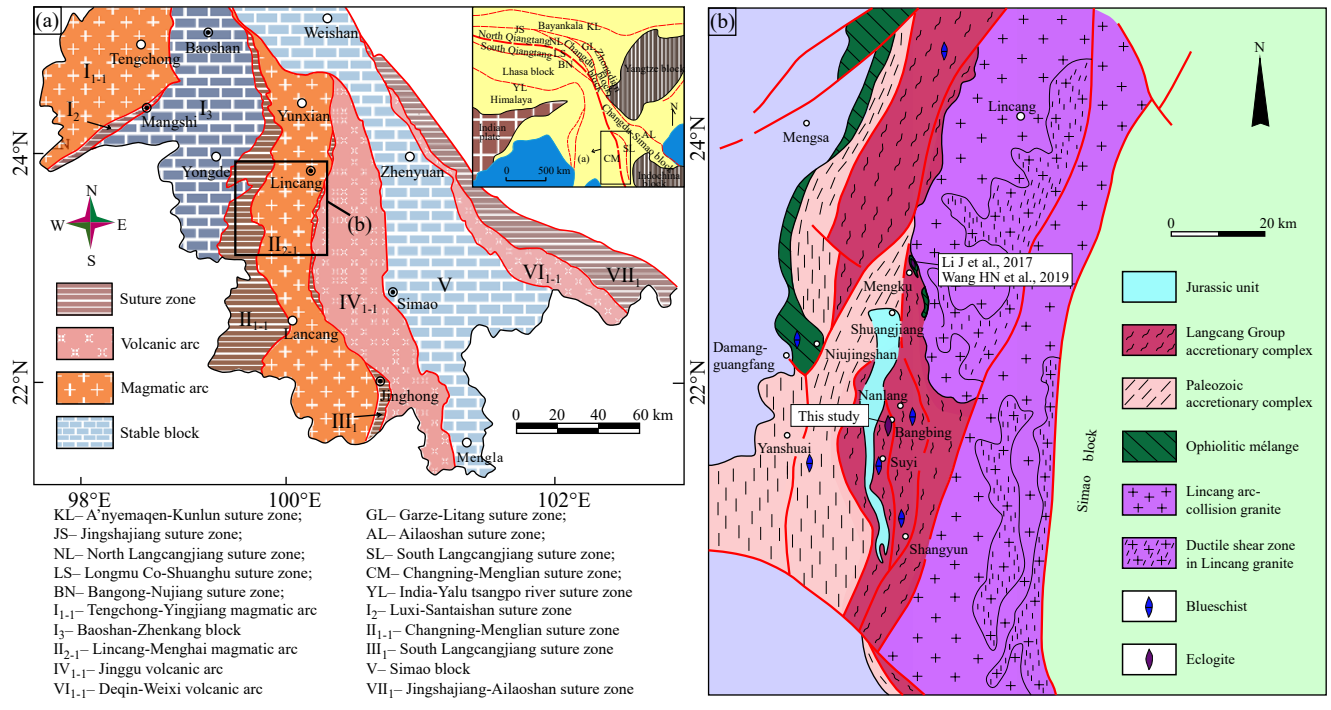

Fig. 1. a–Tectonic location of the Changning-Menglian suture zone (after Wang BD et al., 2018); b–simplified geological map of the Langcang Group accretionary complex in southeast Tibetan Plateau Showing the outcroups of the buleschist and eclogites. The outcroups of the buleshist are from Zhang ZB et al., 2004; Wang F et al., 2016 and Fan WM et al., 2015.

And in some eclogites, garnet is obviously differentiated from omphacite and glaucophane, which shows oriented structure. Actinolite-bearing eclogite feature porphyroblastic texture and massive structure. Porphyroblasts include garnet (30%–40%) and clinozoisite (5%) while the metamorphosed matrix shows needle-shaped granoblastic texture, mainly including omphacite (40%), actinolite (10%), chlorite (5%), quartz (5%) and minor amounts of phengite and rutile. The actinolite-bearing eclogites may be retrograded by the glaucophane eclogites. Mineral abbreviations are after Whitney DL and Evans BW (2010).

5.1. Garnet

Euhedral to subhedral granular texture is shown with sizes ranging from 0.2 mm to 5 mm. Cores of garnet from the glaucophane eclogites are inclusion-rich, containing glaucophane, omphacite, chlorite, rutile, and minor amount of quartz (Figs. 3a–e). The radial cracks around quaretz inclusion shows the possibly retrograde production of coesite (Fig. 3c). Compositional zonation could be observed in the garnet, with the cores of $Alm_{65–70}Prp_{6–11}Grs_{20–23}Sps_{1.0–1.4}$ and the rims of $Alm_{53–62}Prp_{14–18}Grs_{22–28}Sps_{0.4–0.9}$ (Table 1; Figs. 7a–b). From the cores to rims, X_{prp} and X_{grs} increase while X_{sps} and X_{alm} decrease (Fig. 5), showing the prograde growth of the garnet. Compositions of all garnet grains are within the field of type-C high-pressure low-temperature eclogites (Fig. 7a), typical of oceanic eclogites.

Garnet from the actinolite-bearing eclogites are inclusion-poor but compositional zoning also developed (Fig. 4), from the cores as $Alm_{66–68}Prp_{8–10}Grs_{21–22}Sps_{0.9–3.5}$ to the rims as $Alm_{44–50}Prp_{24–30}Grs_{24}Sps_{0.3–0.5}$ (Table 2; Figs. 7a, d). From the cores to rims, X_{prp} and X_{grs} increase while X_{sps} and X_{alm} decrease (Fig. 6), showing the prograde growth of the garnet. Rim compositions of most garnet grains are within the type-C field with only one data point within the field of type-B eclogites whereas all core compositions are within the field of type-C eclogites (Fig. 7a), typical of oceanic eclogites.

5.2. Omphacite

Omphacite in eclogites appears as fresh greenish in color, unaltered, subhedral, stubby, and micro-granular with sizes of about 0.2–0.5 mm. Characteristics of the omphacite from the glaucophane eclogites and actinolite-bearing eclogites are apparently different.

Omphacite in the glaucophane eclogites mainly distributes in the metamorphosed matrix but occurs rarely as inclusions in garnet and clinozoisite. It is apparent that the grain sizes of omphacite in the metamorphosed matrix are larger than those in inclusions (Fig. 3). Compositions of all grains fall within the field of omphacite (Fig. 7c). Corundum contents (X_{Jd}) are relatively low at 0.24–0.33 in the omphacite inclusions (Omp_{-g}) in garnet, with Na/(Na+Ca) ratios of 0.33–0.39. The X_{Jd} are relatively high in omphacite inclusions in clinozoisite at 0.43–0.50, with Na/(Na+Ca) ratios of 0.47–0.54. The X_{Jd} of

Fig. 2. Field occurrence characteristics of eclogites. a, b–beclogites occurring in the shape of lens in the Langcang Group accretionary complex; c, d–hand specimen of the eclogite samples investigated in this study. Grt–garnet; Gln–glaucophane; Omp–omphacite; Czo–clinozosite.

Table 1. Representative major element composition of minerals in glaucophane eclogites.

Mineral	Grt	Grt		Omp	Omp	Omp	Omp		Amp	Amp	Amp	Amp	Amp	Amp	Amp		Ph	Ph		Czo	Czo
Location	Grt-c	Grt-r		Omp_1	Omp_1	Omp_2	Omp_2		Win in Grt	Gln_1 in Grt	Win in Gln	Gln_2	Gln_2	Gln_3	Gln_3		matrix	matrix		Czo-c	Czo-r
SiO_2	38.12	39.30		54.40	55.65	56.13	57.41		54.37	57.32	55.47	57.70	59.29	58.80	58.34		54.26	55.94		39.78	39.75
TiO_2	0.10	0.11		0.05	0.06	0.01	0.05		0.08	0.00	0.10	0.04	0.00	0.06	0.02		0.23	0.13		0.15	0.11
Al_2O_3	20.56	21.57		4.30	6.59	8.96	10.91		3.14	9.53	4.51	8.95	11.40	10.99	10.30		28.40	26.39		30.39	27.11
FeO	31.23	25.34		9.88	5.85	5.97	5.31		13.79	16.03	8.05	9.83	6.40	12.48	12.62		1.30	1.91		5.00	7.51
MnO	0.48	0.17		0.02	0.05	0.00	0.02		0.03	0.11	0.00	0.04	0.01	0.08	0.07		0.00	0.00		0.00	0.04
MgO	1.47	4.68		9.22	10.14	8.54	7.62		14.43	7.67	17.16	11.96	13.38	9.02	9.40		4.15	4.91		0.30	0.09
CaO	7.90	8.83		16.23	15.04	12.96	11.32		9.40	0.53	8.61	2.19	1.65	0.22	0.45		0.00	0.00		23.59	25.03
Na_2O	0.03	0.03		4.38	5.27	6.36	7.32		2.28	5.97	2.70	5.88	6.19	6.37	6.54		0.61	0.28		0.02	0.00
K_2O	0.00	0.02		0.02	0.00	0.00	0.01		0.09	0.00	0.12	0.04	0.01	0.00	0.01		7.52	7.97		0.00	0.02
Total	99.90	100.04		98.49	98.64	98.92	99.98		97.60	97.16	96.70	96.62	98.34	98.01	97.74		96.48	97.53		99.22	99.66
Oxygens	12	12		6	6	6	6		23	23	23	23	23	23	23		11	11		12.5	12.5
Si	3.050	3.049		2.038	2.032	2.030	2.036		7.750	7.971	7.740	7.948	7.862	7.984	7.974		3.467	3.545		3.008	3.030
Ti	0.006	0.006		0.002	0.002	0.000	0.001		0.009	0.000	0.010	0.004	0.000	0.006	0.002		0.011	0.006		0.009	0.006
Al	1.939	1.972		0.190	0.284	0.382	0.456		0.527	1.561	0.741	1.453	1.781	1.758	1.659		2.140	1.971		2.709	2.436
Fe^{3+}	0.000	0.000		0.075	0.033	0.005	0.000		0.438	0.729	0.434	0.420	0.431	0.519	0.524		0.049	0.071		0.283	0.474
Fe^{2+}	2.090	1.644		0.234	0.146	0.176	0.158		1.205	1.136	0.505	0.713	0.279	0.898	0.919		0.021	0.030		0.034	0.005
Mn	0.033	0.011		0.000	0.002	0.000	0.001		0.004	0.013	0.000	0.005	0.001	0.009	0.008		0.000	0.000		0.000	0.003
Mg	0.176	0.541		0.515	0.552	0.460	0.403		3.067	1.591	3.570	2.457	2.646	1.825	1.915		0.396	0.464		0.034	0.010
Ca	0.677	0.734		0.651	0.589	0.502	0.430		1.435	0.080	1.286	0.323	0.235	0.032	0.066		0.000	0.000		1.911	2.044
Na	0.005	0.004		0.318	0.373	0.446	0.503		0.630	1.609	0.730	1.569	1.591	1.678	1.733		0.075	0.035		0.003	0.000
K	0.000	0.002		0	0	0	0		0.016	0.000	0.022	0.007	0.002	0.000	0.001		0.613	0.644		0.000	0.002
Sum	8.00	8.00		4.00	4.00	4.00	4.00		15.08	14.69	15.04	14.90	14.83	14.71	14.80		6.77	6.77		7.99	8.01
Alm	69.67	54.79	WEF	0.69	0.63	0.56	0.50	Al^{IV}	0.250	0.029	0.260	0.052	0.138	0.016	0.026	X_{Na}'	0.11	0.05	Ps	0.09	0.16
Grs	22.57	24.46	Jd	0.24	0.33	0.43	0.50	Al^{VI}	0.277	1.532	0.481	1.401	1.643	1.743	1.633	X_{Fe}	0.05	0.06			
Prp	5.86	18.04	Ae	0.07	0.03	0.00	0.00	Na_B	0.565	1.920	0.714	1.677	1.765	1.968	1.934						
Sps	1.09	0.37	X_{Na}	0.33	0.39	0.47	0.54	X_{Mg}	0.72	0.58	0.88	0.78	0.90	0.67	0.68						

Notes: Alm–almandine; Grs–grossular; Prp–pyrope; Sps–spessartine; WEF–wollastonite+enstatite+ferrosilite; Jd–jadeite; Ae–aegirine; Amp–amphibole; Ph–phengite; other symbols are shown in Fig. 2. X_{Na}=Na/(Na+Ca); X_{Mg}=Mg/(Mg+Fe^{2+}); X_{Na}'=Na/(Na+K); X_{Fe}=Fe^{2+}/(Fe^{2+}+Mg); Ps=Fe^{3+}/(Fe^{3+}+Al); c–core region of mineral; r–rim region of mineral; Fe^{3+} was caculated assuming stoichiometric mineral compositions.

Table 2. Representative major element composition of minerals in actinolite eclogites.

Mineral	Grt	Grt		Omp	Omp		Amp	Amp		Ph	Ph		Czo	Czo
Location	Grt-c	Grt-r		Omp_3	Omp_3		Act	Act		matrix	matrix		Czo-c	Czo-r
SiO_2	37.79	40.25		56.86	56.71		56.37	56.51		54.06	55.80		39.57	39.89
TiO_2	0.18	0.00		0.00	0.00		0.00	0.04		0.27	0.15		0.18	0.05
Al_2O_3	20.65	22.19		7.51	9.42		4.02	1.77		28.25	25.32		30.34	29.18
FeO	30.41	20.60		4.23	2.77		6.02	8.38		1.39	1.53		5.11	6.08
MnO	1.06	0.15		0.11	0.07		0.05	0.11		0.01	0.01		0.00	0.03
MgO	1.97	8.10		10.99	9.55		18.31	18.40		4.79	5.34		0.32	0.11
CaO	7.43	8.78		16.63	15.18		11.37	11.48		0.00	0.04		25.15	25.58
Na_2O	0.01	0.01		4.38	5.38		1.71	1.59		0.46	0.35		0.02	0.00
K_2O	0.00	0.00		0.00	0.04		0.11	0.06		7.42	7.46		0.00	0.02
Total	99.50	100.09		100.70	99.12		97.95	98.34		96.64	96.00		100.68	100.94
Oxygens	12	12		6	6		23	23		11	11		12.5	12.5
Si	3.031	3.046		2.018	2.023		7.805	7.886		3.450	3.580		2.964	2.992
Ti	0.011	0.000		0.000	0.000		0.000	0.004		0.013	0.007		0.010	0.003
Al	1.953	1.979		0.314	0.396		0.656	0.291		2.125	1.915		2.680	2.580
Fe^{3+}	0.000	0.000		0.000	0.000		0.000	0.057		0.052	0.058		0.310	0.378
Fe^{2+}	2.040	1.304		0.126	0.083		0.697	0.921		0.022	0.025		0.010	0.004
Mn	0.072	0.010		0.003	0.002		0.006	0.013		0.000	0.001		0.000	0.002
Mg	0.235	0.913		0.581	0.508		3.779	3.828		0.455	0.510		0.036	0.012
Ca	0.639	0.712		0.632	0.580		1.686	1.716		0.000	0.003		2.019	2.056
Na	0.002	0.001		0.301	0.372		0.458	0.429		0.056	0.044		0.003	0.000
K	0.000	0.000					0.020	0.011		0.604	0.610		0.000	0.002
Sum	8.00	8.00		4.00	4.00		15.11	15.16		6.78	6.75		8.032	8.029
Alm	68.00	43.46	WEF	0.69	0.61	Al^{IV}	0.195	0.114	X_{Na}'	0.08	0.07	Ps	0.10	0.13
Grs	21.30	23.74	Jd	0.31	0.39	Al^{VI}	0.461	0.177	X_{Fe}	0.05	0.05			
Prp	7.85	30.44	Ae	0.00	0.00	Na_B	0.314	0.284						
Sps	2.39	0.33	X_{Na}	0.32	0.39	X_{Mg}	0.84	0.81						

Notes: All the abbreviations as the same as the Table 1.

omphacite in the metamorphosed matrix are similar to those included in clinozoisite (Table 1; Fig. 7c). From microscopic observation, the boundaries between omphacite and garnet in the metamorphosed matrix are flat and straight, showing that they are in equilibrium intergrowth, whereas the boundaries with clinozoisite are embayed (Fig. 3i), indicating that clinozoisite is likely a post-peak retrograde mineral. Therefore, both omphacite in the metamorphosed matrix and as inclusions in clinozoisite were the products of peak metamorphism, formed slightly later than those included in garnet, and could be classified as peak-stage omphacite .

Omphacite in the actinolite-bearing eclogites mainly developed in the metamorphosed matrix and rarely occurs as inclusions in clinozisite (Fig. 4). Although garnet is common in this type of rock, omphacite inclusions in garnet have not been observed. Compositions of omphacite in the metamorphosed matrix and as inclusions of clinozisite are the same, with X_{Jd} of 0.31–0.39, and Na/(Na+Ca) ratios of 0.32–0.39 (Table 2; Fig. 7c). X_{Jd} of this type of omphacite are between those of Omp_{-g} and Omp in matrix of glaucophane eclogites.

5.3. Amphibole group minerals

Amphibole group minerals are euhedral to subhedral in shape with various grain sizes. Most grains occur as porphyroblasts and minor amount occurs in metamorphosed matrix or as inclusions in garnet. Clear optical and compositional zonation is observed. Chemical formula of the amphibole group minerals were calculated following Leake BE et al. (1997).

Inclusions of amphibole group minerals in garnet are mainly crossite (Figs. 3e, 7f). Occasionally winchite (Wnc_{-g}) is observed in the cores of crosstie ($G1n_{-g}$) and from Wnc_{-g}→Gln_{-g}, contents of Al_2O_3 and Al^{VI} apparently increase from 3.14% to 9.53% and from 0.277 p.f.u to 1.532 p.f.u. respectively, but Al^{IV}contents and X_{Mg}[Mg/(Fe^{2+}+Mg)] decrease from 0.250 p.f.u to 0.029 p.f.u. and from 0.72 to 0.58 respectively (Table 1).

The amphibole group mineral occurring as porphyroblasts and in the metamorphosed matrix is mainly glaucophane (Figs. 2a, f–h, Fig. 7e, f) and there are three types of zonation patterns. (1) Glaucophane containing the winchite inclusion (Wnc_{-gl}→Gln); Al^{VI} contents increase and X_{Mg} decrease from core to rim in term of chemical composition (Table 1). (2) Cores of light blue glaucophane and rims of dark blue glaucophane (Gln_1→Gln_2) (Fig. 3a, g); this is the most common type of zonation. Gln_1 and Gln_2 have similar major element compositions, but Gln_1 has slightly higher MgO contents (11.96 %–13.38 %), Al^{IV} contents (0.052–0.138 p.f.u.) and X_{Mg} (0.78–0.90), but lower FeO contents (6.40 %–9.83 %) in the core than Gln_2 (MgO contents of 9.02%–9.40%, Al^{IV} contents of 0.016–0.026 p.f.u., X_{Mg} of 0.67–0.68 and FeO contents of 12.48%–12.62%) (Table 1; Fig. 7f). These show

that the formation temperature of the rim Gln_2 is lower than the core Gln_1 and the rims occur as retrograde metamorphic bands. (3) In the composite zonation of the former two types, from the center to the rim, minerals underwent the following textural transition: Arg→Gln_1→Gln_2 and Wnc_{-gl}+Gln_1→Gln_2 (Figs. 3f–h).

The amphibole in actinolite-bearing eclogites with Si contents of 7.805–7.886 p.f.u. and Na_B contents of 0.284–0.314 p.f.u. is classified as actinolite (Table 2; Fig. 7e). Actinolite may be formed by retrograded glaucophane.

5.4. Phengite

Phengite occurs as sheets in the metamorphosed matrix and mainly appears interstitial to omphacite grains with flat and straight boundaries, indicating that phengite is the product of peak metamorphism. Phengite in glaucophane eclogites have Si contents of 3.467–3.545 p.f.u., X_{Na} [Na/(Na+K)] from 0.05 to 0.11, and X_{Fe} [Fe^{2+}/(Fe^{2+}+Mg)] ranging from 0.04 to 0.15 (Table 1). Phengite in actinolite-bearing eclogites shows similar contents of Si (3.450–3.580 p.f.u.), X_{Na} (0.07–0.08)

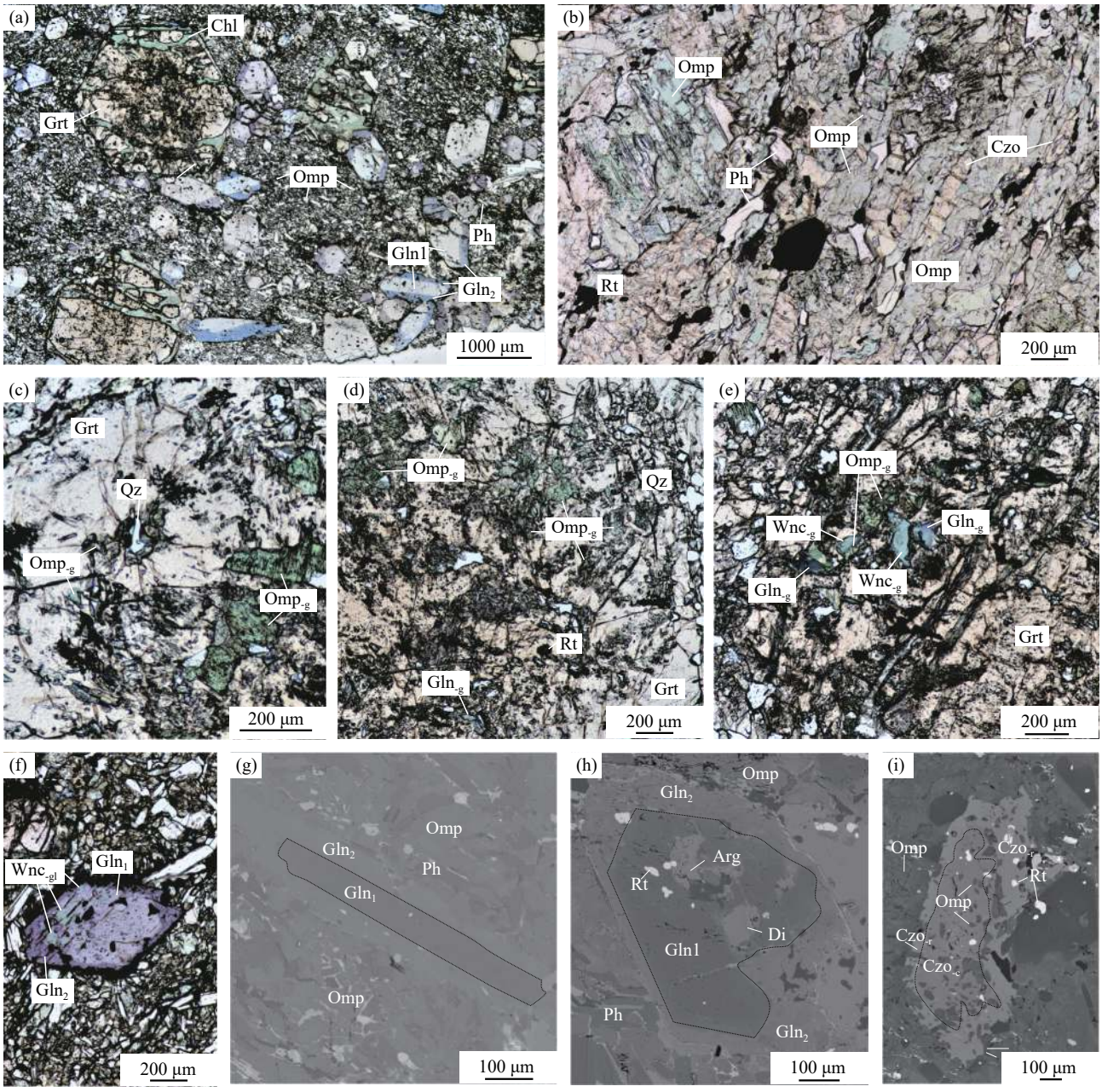

Fig. 3. Photomicrographs and Backscattered-electron(BSE) images showing the textural relationship of glaucophane eclogite. a–The glaucophane eclogite with mineral assemblage of garnet+omphacite+glaucophane +phengite, and chlorite distributes surrounds garnet, in plane-polarized light (PPL); b–omphacite from the glaucophane eclogites in matrix and its paragenetic mineral (PPL); c–e–porphyroblastic garnet from the glaucophane eclogites showing various inclusions of omphacite (Omp_{-g}), winchite (Wnc_{-g}), glaucophane (Gln_{-g}), quartz and rutile (PPL), and the radial cracks around quaretz inclusion showing the possibly retrograde production of coesite (c); f–h–representative structures showing the zonation of glaucophane, winchite and other mineral (Di, Arg→Gln_1→Gln_2 and Win-g, Gln_1→Gln_2), f is in PPL and g–h is BSE image; i–BSE image of omphacite from the glaucophane eclogite in clinozoisite, which showing apparent optical zonation. Arg –aragonite; Chl –chlorite; Di–diopside; Rt–rutile; other symbols are shown in Fig.2.

and relatively low contents of X_{Fe}(0.05) (Table 2), typical of those formed under HP/UHP metamorphic conditions (Grimmer JC et al., 2003).

5.5. Otherminerals

Epidote in the eclogites is clinozoisite, occurring as porphyroblasts with inclusions of omphacite and rutile, and showing apparent optical and compositional zonation (Fig. 3i). In glaucophane eclogites, the contents of Al_2O_3 decrease from 30.39% to 27.11%, while the contents of FeO^T and the X_{Ps} [Fe^{3+}/(Fe^{3+}+Al)] ratios increase from 4.52% to 7.51% and from 0.09 to 0.16, respectively, from cores to rims of clinozoisite (Table 1). In actinolite-bearing eclogites, the contents of Al_2O_3 decrease from 30.34% to 29.18%, while the contents of FeO^T and the X_{Ps} ratios increase from 5.11% to 6.08% and from 0.10 to 0.13, respectively, from cores to rims of clinozoisite (Table 2).

Rutile grains occur as needle- or irregular-shaped and mainly in the metamorphosed matrix, with a minor amount as inclusions in garnet, omphacite, glaucophane, and clinozoisite. Occasionally, retrograded rutile to titanite is observed.

Quartz commonly occurs in metamorphosed matrix or as inclusions in porphyroblasts. In metamorphosed matrix, quartz grains are usually relatively concentrated to form aggregate. Chlorite usually distributes along fractures of garnet grains or surrounds garnet grains to show circular and

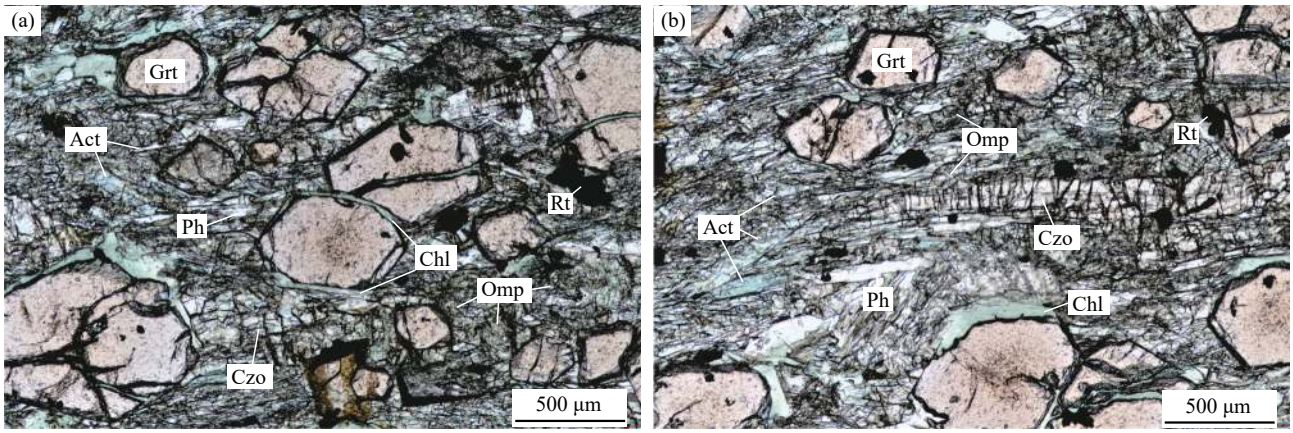

Fig. 4. Microscopic characteristics of the actinolite-bearing eclogite. The eclogite with mineral assemblage of garnet (Grt) + omphacite (Omp) + actinolite (Act) + phengite (Ph) + clinozoisite (Czo), and chlorite (Chl) distributes surrounds garnet. The actinolite (Act) may be retrograded by the glaucophane (PPL).

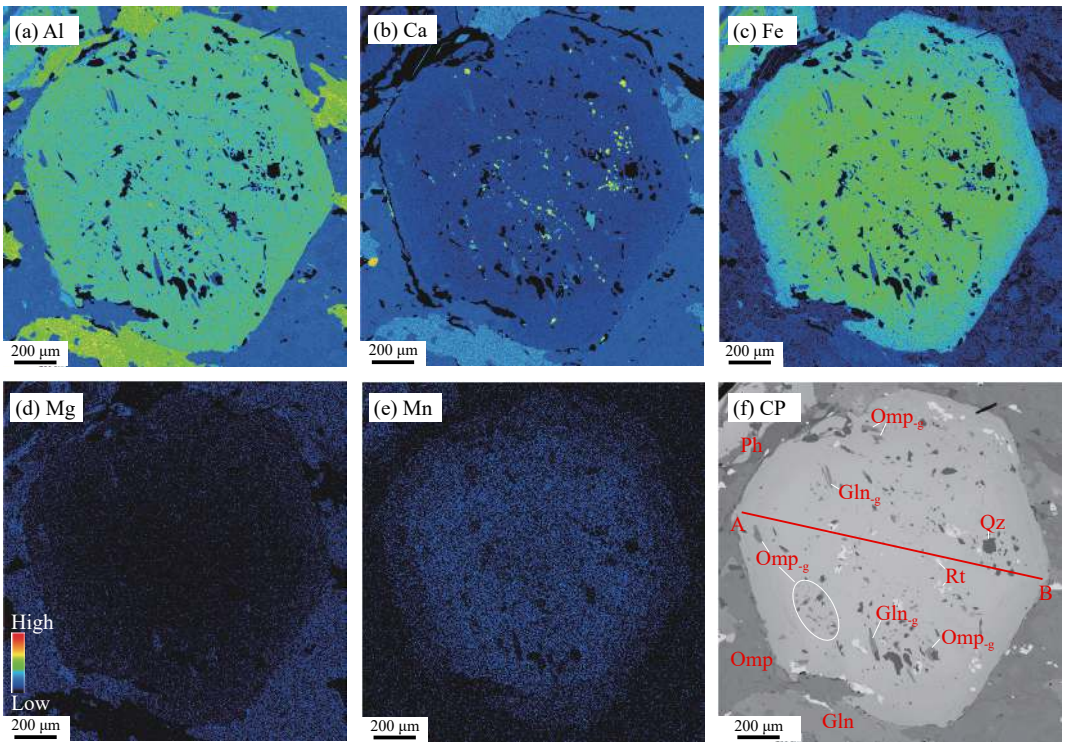

Fig. 5. Element X-ray maps (a–e) and BSE image (f) of garnet in the glaucophane eclogite. The euhedral garnet crystal reveals a zonation and contains inclusions of omphacite (Omp$_{-g}$), glaucophane (Gln$_{-g}$), quartz (Qz) and rutile.

banded pattern, forming the symplectite structure (Figs. 3a, 4).

6. Metamorphic evolution and *P-T* paths

The textural observations and mineral compositions described above, four stages of metamorphic mineral growth are distinguished. The textures and mineral assemblages of each metamorphic stage are described below: The prograde stage of metamorphism (M_1), the peak stage of metamorphism (M_2), the post-peak stage of metamorphism (M_3), and the last stage of metamorphism (M_4; Fig. 8).

The prograde stage of metamorphism (M_1) in the glaucophane eclogites is represented dominantly by the formation of garnet (core) and the abundant inclusions in the HP mineral pahases (Fig. 8). The garnet core compositions that constrain the assemblage Grt_C + Omp_{-g}(X_{Jd}=0.24–0.33) + Gln_{-g} + Arg + Qz + Rt suggest that the eclogites form the Bangbing area underwent a blueschist facies metamorphism prior to the eclogite facies metamorphism (Fig. 9). The absence of early stage phengite could be due to the omphacite/crossite at its expense. Hence, garnet-clinopyroxene (GC) geothermometer (Ravna K, 2000) and garnet-clinopyroxene ($GC^{\#}$) geobarometer (Beyer C et al., 2015) were adopted to estimate the *P-T* conditions of this stage. Core compositions of garnet grains (of the highest X_{Mn} and the lowest X_{Mg}) were used in the calculation. Pressures of 2000–2310 MPa (average 2150 MPa), and temperatures of 407–480°C (average 452°C) were obtained for eclogites from the Bangbing area, falling within the transitional field of blueschist facies and eclogite facies (the bule diamond; Fig. 9).

Further subduction moved the eclogites into the field of lawsonite-eclogite facies (M_2). This is defined by the rims of porphyroblastic garnet grains with maximum pyrope and gross ular contents, the occurrence of metamorphosed matrix omphacite (Omp) with maximum X_{Jd}, and maximum Si contents in phengite inclusions. At this stage, the eclogites have been subducted to the deepest and experienced a certain period of residence and heating before exhumation, leading to the peak metamorphism. The mineral assemblage of this stage of metamorphism is Grt(rim)+Omp (X_{Jd}=0.43–0.50, 0.32–0.39) +Gln_1 + Lws? + Ph ± Qz + Rt. As the omphacite formed during the peak metamorphism has X_{Jd}<0.55, the rim compositions of the garnet grains (of the highest X_{Mg} and X_{Ga}) and chemical compositions of the synchronous omphacite (of the highest X_{Jd}) and phengite (of the highest Si contents) were adopted (Table 1). Using the garnet-clinopyroxene Fe^{2+}-Mg exchange geothermometer of Ravna K (2000) and garent-clinopyroxene-phengite geobarometer (Ravna EJK and Terry MP, 2004; Chen Y et al., 2005) for the calculation, the *P-T* conditions of the peak metamorphism of the eclogites were 3000–3270 MPa (average 3060 MPa) and 617–658°C (average 630°C), within the field of lawsonite-eclogite facies (law-EC) (the blue circles; Fig. 9). Such condition apparently exceeded the pressure for phase transition from quartz to coesite (2800 MPa ±), which is consistent with the radial

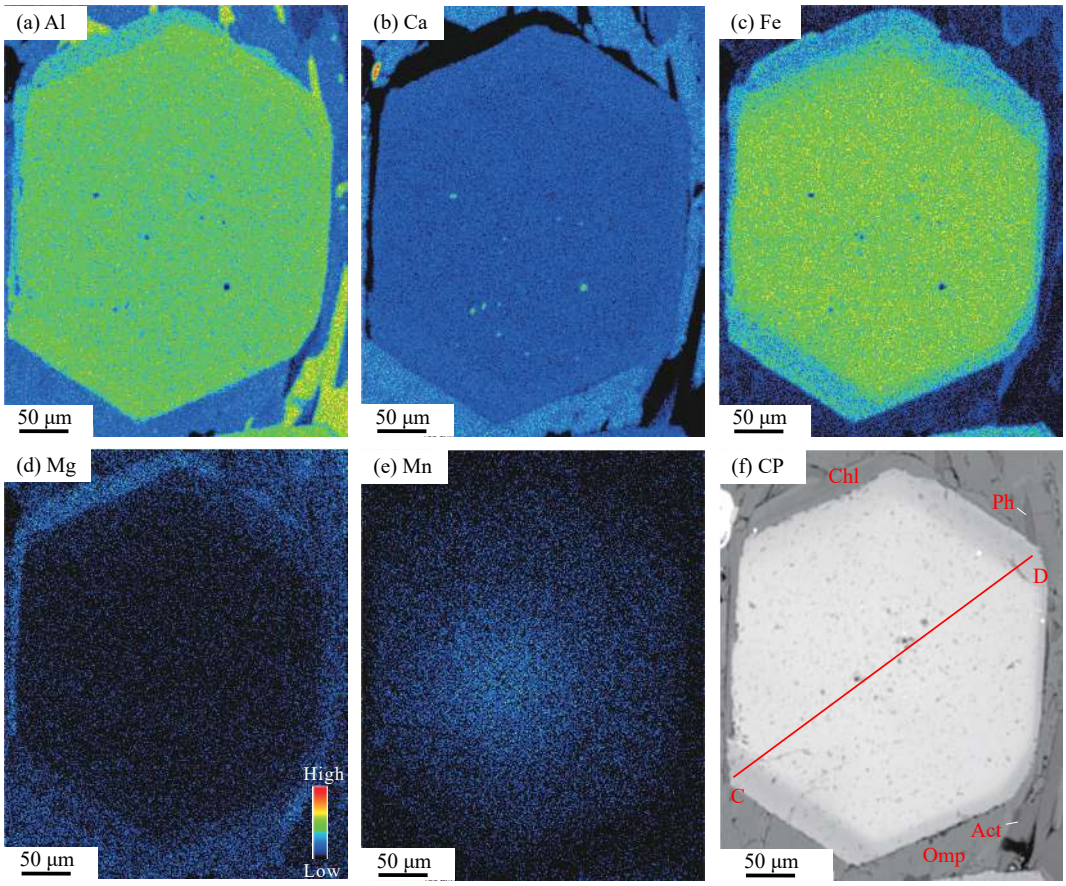

Fig. 6. Element X-ray maps (a–e) and BSE image (f) of garnet in the actinolite-bearing eclogite showing a zonation and poor inclusion.

cracks around quartz inclusions of the garnet edge, implying an ultrahigh-pressure metamorphism of this stage. However, further works are needed to identify minerals that represent ultrahigh-pressure conditions.

After the peak metamorphism, the eclogites started to exhume and characterized by the formation of mineral assemblage including retrograded glaucophane (Gln_2), winchite ($Wnc_{-g/gl}$), phengite, clinozoisite, minor actinolite,

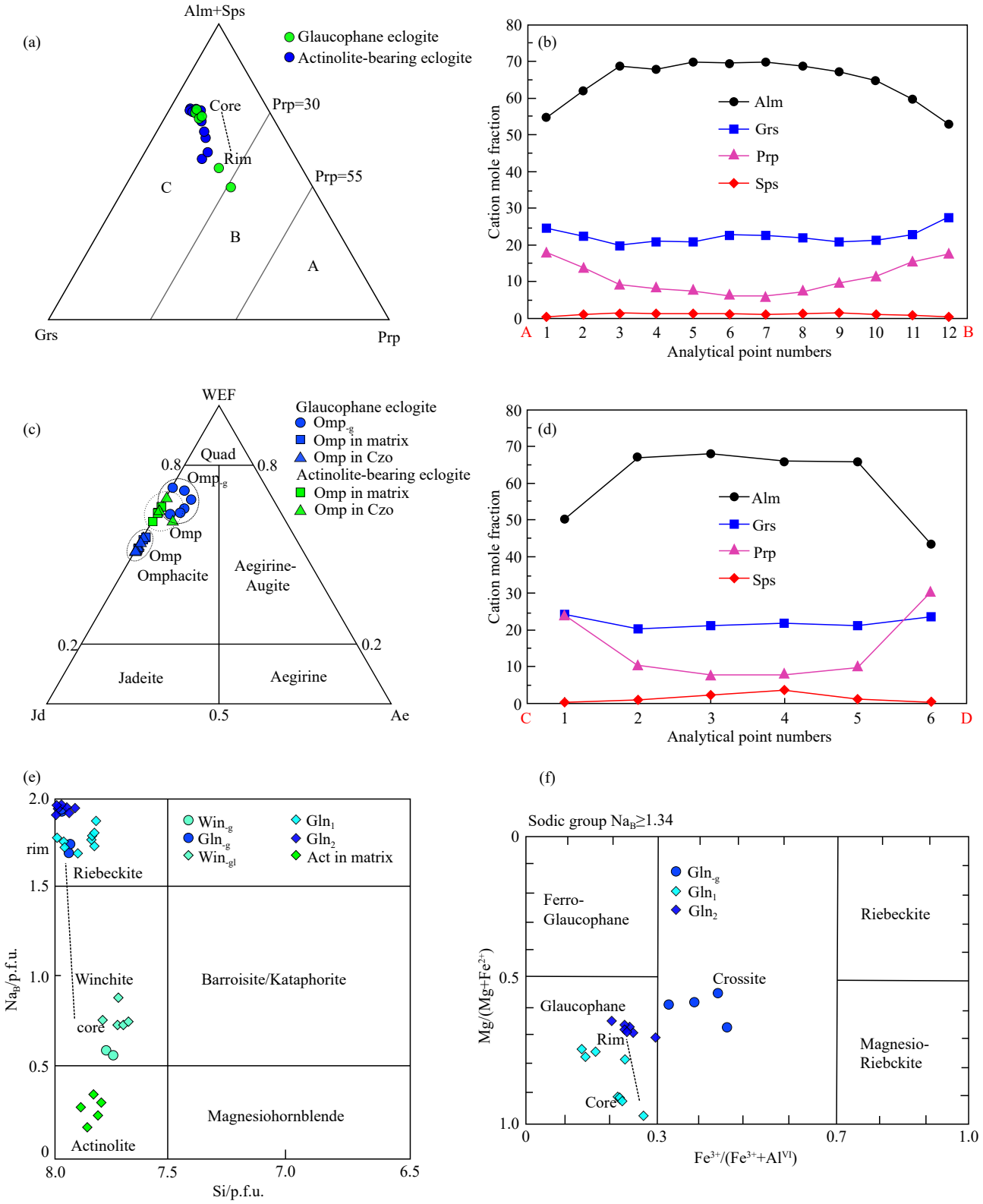

Fig. 7. Chemical compositions of garnet, omphacite and amphibolite in the eclogite: a–teranry plot of (alm+sps)-grs-prp of garnet compositions (after Coleman R et al., 1965); b, d–compositional profile intersecting the center of the garnet porphyroblast in Fig. 5f and Fig. 6f showing the prograde growth both; c–ternay classification diagram for sodic clinopyroxenes after Morimoto N et al. (1988); e, f–chemical composition of amphibolite in the eclogite after Leake BE et al. (1997).

and rutile (M_3). In the early stage of exhumation, glaucophane (Gln_{-g} and Gln_1) was replaced or rimmed by winchite. The increase in Al^{IV} contents and X_{Mg} from Gln to Wnc suggest that the temperature rises briefly in the early stage of

Stages	M_1	M_2	M_3	M_4
Garnet	Grt_c	Grt_r		
Omphacite	Omp_{-g} X_{Jd}=0.24−0.33	Omp X_{Jd}=0.32−0.39, 0.43−0.50		
Diopside				
Amphibole	Gln_{-g}	Gln_1	Gln_2 + $Wnc_{-g/gl}$	Act
Phengite	?			
Lawsonite	?	?		
Aragonite				
Clinozoisite			Czo_{-c}	Czo_{-r}
Rutile				
Titanite				
Biotite/Chlorite				
Quartz				

Fig. 8. Mineral assemblages and compositions during metamorphic evolutions.

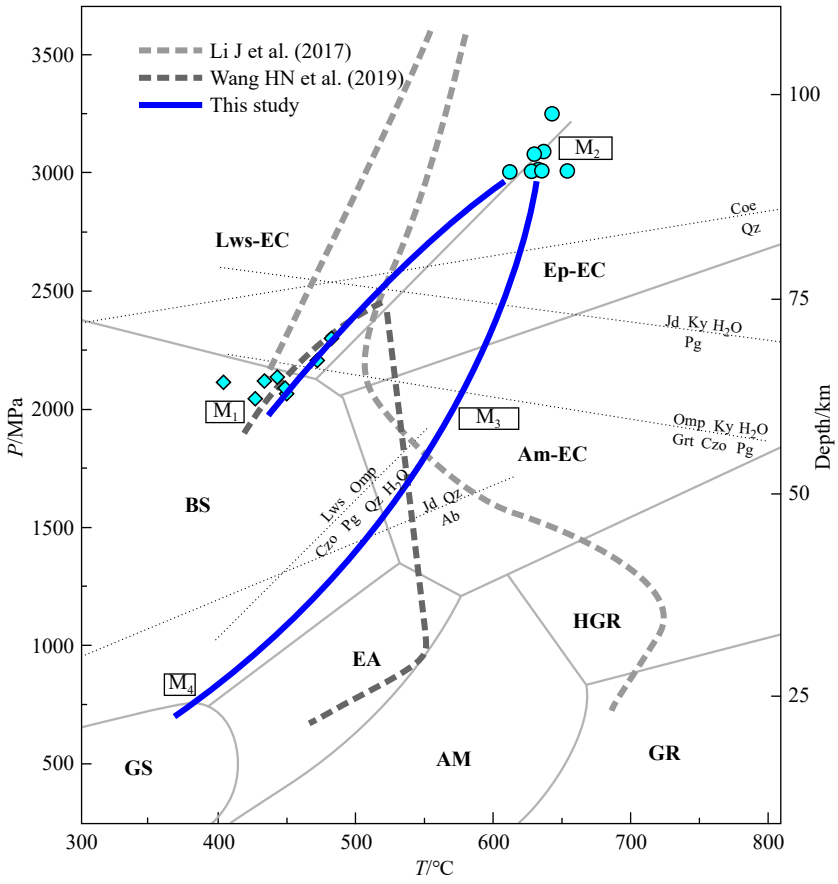

Fig. 9. *P-T* path for the eclogites in the Bangbing (blue arrow) and Mengku area (gray arrow). The bule diamond are *P-T* data estimated based on the geothermometer of Ravna K (2000) and geobarometer of Beyer C et al. (2015); the blue circles are the *P-T* data estimated based on the geothermometer of Ravna K (2000) and geobarometer of Ravna EJK and Terry MP (2004). The metamorphic facies and their abbreviations follow Liou JG et al. (2004) and Zhai QG et al. (2011b). Lws-EC–lawsonite-eclogite facies; Ep-EC–epidote-eclogite facies; Am-EC–amphibole-eclogite facies; BS–blueschist facies; EA–epidote amphibolite facies; AM–amphibolite facies; HGR–high granulite facies; GR–granulite facies; GS–greenschist facies.

exhumation. This indicates a short period of heating of the eclogites after the peak pressure, which may be related to the "thermal relaxation" experienced by the rocks during the early stage of exhumation (Li JL et al., 2012; Du JX et al., 2014). Exhumation accelerated afterward and during this process, glaucophane (Gln_2), clinozoisite, and actinolite formed. Glaucophane of this stage has apparent optical and compositional zonation with MgO and Al^{IV} contents decreasing while FeO contents increasing from cores (Gln_1) to rims (Gln_2) of bands. The decrease in Al^{IV} contents implies that the rims of glaucophane grains formed at a lower temperature (Genshaft YS and Mironova NA, 1995; Dong YL et al., 2016), whereas the variations in MgO and FeO contents may resemble the Fe-Mg re-exchange process in garnet during cooling (Xia QY and Zheng YF, 2011). Such cooling was also recorded and exhibited in the country rocks (blueschists) of the eclogites (Fan WM et al., 2015). The metamorphism of this stage during exhumation is non-equilibrium, and the *P-T* conditions are difficult to calculate. The retrograded assemblage of glaucophane, clinozoisite, and actinolite reveals that the retrograde metamorphism of the eclogites may enter the epidote amphibolite facies to blueschist facies (Fig. 9).

The last stage (retrograde greenschist facies) is defined by euhedral actinolite and titanite in the matrix, diopside inclusions of glaucophane, and chlorite overgrowths on garnet (M_4; Fig. 9). Brittle deformation took place on garnet porphyroblasts whereas actinolite and chlorite might be formed by retrograded glaucophane and biotite respectively. The emergence of the last stage phases indicate that the eclogites have been exhumed to shallow depth in the crust.

7. Discussion

7.1. Metamorphic evolution of glaucophane eclogites

Glaucophane eclogites form in environments of relatively low temperature gradient and occur as products in subduction of cold oceanic crust (Carson CJ et al., 1999; Zhang LY et al., 2008; Wei CJ et al., 2010). The formation and evolution of glaucophane eclogites reflect, to a certain degree, the evolutionary process of the ocean basins. The discovery of eclogites at the Bangbing area of the Changning-Menglian suture zone has very important tectonic significance to understand the deep subduction and exhumation of the Paleo-Tethys Ocean.

According to petrographic observation and estimation by geothermo-barometers, lawsonite should commonly occur in the prograde metamorphic stage, peak metamorphism and early exhumation of the Bangbing eclogites. Yet, lawsonite is not observed in the rock samples and the occurrence is even pseudo. Indeed, this paradox exists for many eclogites (Clarke GL et al., 2006; Tsujimori T et al., 2008; Wei CJ and Clarke GL, 2011). During exhumation, substantial dehydration of lawsonite would form epidote or clinozoisite, and hence, lawsonite was difficult to preserve (Clarke GL et al., 2006; Wei CJ and Clarke GL, 2011). It is likely that lawonsite had experienced dehydration and transformed to clinozoisite, and hence not preserved in early decompressional metamorphic process. Evidence includes the discovery of lawsonite inclusions in garnet of retrograded eclogites in the Mengku region (Li J et al., 2017; Wang HN et al., 2019), inclusions of omphacite from the peak metamorphism in clinozoisite, and retrograded bands in clinozoisite grains of the Bangbing eclogites. Therefore, the mineral assemblage during the peak metamorphism of the glaucophane eclogites is likely garnet (Grt)+omphacite (Omp)+phengite (Ph)+lawsonite (Law)+rutile (Rt), with the *P-T* conditions of 3000–3270 MPa and 617–658°C. The probable occurrence of lawsonite and stable and widespread occurrence of glaucophane in the rocks indicate lower metamorphic temperatures, and hence, the rocks could be classified as low-temperature ultrahigh-pressure eclogites (Zhang LF et al., 2008; Wei CJ et al., 2013). The rocks have experienced metamorphism at blueschist facies during the prograde metamorphism under a low geothermal gradient characterized of a cold subduction. It proves that the Bangbing eclogites may represent a new oceanic HP to UHP metamorphic belt in the Changning-Menglian suture zone.

7.2. Implications for the subducion of the Paleo-Tethyan oceanic plate

The Bangbing glaucophane eclogites expose in the blueschist metamorphic belt of the Lancang Group characterized by accretionary mélange, whereas the lawsonite-bearing retrograded eclogites in the Mengku area expose at the northeast in the Wanhe ophiolitic complex between the Lancang Group and the Lincang arc granites. Two suites of eclogites have a distance of about 80 km and both are located in the Changning-Menglian suture zone (Fig. 1b), occurring as tectonic mélange. Both glaucophane eclogites and lawsonite-bearing retrograded eclogites belong to oceanic low-temperature HP/UHP eclogites (Li J et al., 2017; Wang HN et al., 2019, Wang HN et al., 2020b and this study). The retrieved metamorphic *P-T* paths of both Bangbing eclogites and Mengku retrograded eclogites are clockwise (Fig. 7), and recorded the subduction of the oceanic lithosphere and post-convergence arc-continent collision and exhumation. Both eclogite suites have experienced prograde metamorphism from lawsonite-blueschist facies to lawsonite-eclogite facies, but the peak metamorphic *P-T* conditions vary, as well as the retrograde metamorphic paths. The Mengku retrograded eclogites have experienced retrograde metamorphism from epidote-eclogite facies to amphibolite facies to form the present garnet amphibolites, with residual omphacite occurring as inclusions in garnet or other retrograde minerals in the late stage (Li J et al., 2017; Wang HN et al., 2019). Whereas retrograde metamorphism of the Bangbing eclogites occurred from the epidote-glaucophane-eclogite facies to blueschist facies, with preservation of abundant fresh omphacite and glaucophane in the metamorphosed matrix. Both two eclogite suites are located in

the same tectonic suture zone and expose as tectonic lenses in accretionary and ophiolitic complexes, but they have experienced different metamorphic *P-T* paths. These rocks may have recorded the processes in an ancient subduction channel along the plate boundary between the overriding and downgoing plates (Cloos M and Shreve RL, 1988). The eclogite blocks detached from the subducting oceanic plates may exhume from different depths, or from different parts of the subducting oceanic crust, and hence, the exhumed eclogite blocks often show various peak *P-T* conditions and different *P-T* paths (Krebs M et al., 2011; Zheng YF et al., 2013; Klemd R et al., 2015). Continuous exhumation of rock blocks along the channel flow would cause the concentration of the peak metamorphic ages of the eclogites into a certain period of time (Guillot S et al., 2009). The peak metamorphic ages of the Mengku retrograded eclogites and the blueschists surrounding the Bangbing eclogites are 246–245 Ma (Wang HN et al., 2019) and 229 Ma (Ar-Ar age of glaucophane, unpublished data from the research group) respectively. The difference in metamorphic ages between the two is 17 Ma. Considering the abundant zircon U-Pb ages of 230–210 Ma for the post-collisional granites in the Lincang magmatic arc to the east of the suture zone (Peng TP et al., 2006; Fan WM et al., 2009; Kong HL et al., 2012) that are about 10 Ma different to the peak metamorphic ages during subduction of the high-pressure metamorphic rocks, the process of exhumation was relatively short with higher rates that might reach 3–6 mm/a (Li JL et al., 2016b). This is consistent with the petrographic feature that abundant preservation of fresh omphacite and glaucophane in the Bangbing eclogites. It has been suggested that all these features may be characteristics of global subduction channels (Kusky TM et al., 1997; Li JL et al., 2016a).

8. Conclusions

(i) In the Changning-Menglian suture zone at the southeastern Tibetan Plateau, fresh glaucophane eclogites were newly discovered. The eclogites occur as tectonic lenses in the blueschist metamorphic belt of the Lancang Group characterized by accretionary mélange. The mineral assemblage of the peak metamorphism is Grt+Omp+Ph+Law±Qz+Rt with the peak *P-T* conditions at 3000–3270 MPa and 617–658°C. Four stages of metamorphism were identified and glaucophane formed during the prograde and retrograde metamorphism. The eclogites could be classified as oceanic low-temperature ultrahigh-pressure eclogites. *P-T* paths of the glaucophane eclogites completely recorded the deep subduction and rapid exhumation of the Triassic Changning-Menglian Ocean.glian Ocean.

(ii) Both the Bangbing glaucophane eclogites and Mengku lawsonite-bearing retrograded eclogites are located in the same tectonic suture zone and expose as tectonic lenses in accretionary and ophiolitic complexes respectively. Yet, the two eclogite suites have different mineral assemblages and have experienced different metamorphic *P-T* paths. These differences indicate that the HP/UHP metamorphism occurred at different depths or different localities in the subduction channel formed during subduction of the Triassic Changning-Menglian Ocean, and exhibit as tectonic accretion after subsequent rapid exhumation.

(iii) Comparable the metamorphic evolution process of two different types eclogites in Bangbing and Mengku area show that an oceanic HP-UHP metamorphic belt in the Changning-Menglian suture zone. This oceanic belt provides an important evidence for further exploring the subduction and collision tectonic evolution process of the Changning-Menglian Paleo-Tethys Ocean.

CRediT authorship contribution statement

Yu-zhen Fu and Zhi-ming Peng conceived of the presented idea. Yu-zhen Fu, Zhi-ming Peng and Guo-zhi Wang wrote the manuscript in consultation. Zhi-ming Peng, Bao-di Wang and Guo-zhi Wang supervised the finding of this work. Jing-feng Hu, Jun-lei Guan, Ji Zhang, Zhang Zhang, Yun-he Liu and Zou Hao contributed to sample preparation and helped supervise the project. All authors discussed the results and contributed to the final manuscript.

Declaration of competing interest

The authors declare no conflicts of interest.

Acknowledgment

This study was supported by the National Natural Science Foundation of China (92055314 and 41602091) and the geological survey project of China Geological Survey (DD20160016).

References

Bao P, Xiao X, Wang J, Li C, Hu K. 1999. Studies on the blueschist belt in the Shuanghu region, central northern Tibet and its tectonic implications. Continental Dynamics, 2, 51–64.

Beyer C, Frost DJ, Miyajima N. 2015. Experimental calibration of a garnet-clinopyroxene geobarometer for mantle eclogites. Contributions to Mineralogy and Petrology, 169(2), 1–21. doi: 10.1007/s00410-015-1113-z.

Carson CJ, Powell R, Clarke GL. 1999. Calculated mineral equilibria for eclogites in CaO-Na_2O-FeO-MgO-Al_2O_3-SiO_2-H_2O: Application to the Pouébo Terrane, Pam Peninsula, New Caledonia. Journal of Metamorphic Geology, 17(1), 9–24. doi: 10.1046/j.1525-1314.1999.00177.x.

Chen Y, Ye K, Wu CM. 2005. Reviews on applying common-used geothermobarometers for eclogites. Acta Petrologica Sinina, 21(4), 1067–1080 (in Chinese with English abstract).

Clarke GL, Powell R, Fitzherbert JA. 2006. The lawsonite paradox: A comparison of field evidence and mineral equilibria modelling. Journal of Metamorphic Geology, 24(8), 715–725. doi: 10.1111/j.1525-1314.2006.00664.x.

Cloos M, Shreve RL. 1988. Subduction-channel model of prism accretion, melange formation, sediment subduction, and subduction erosion at convergent plate margins: 2. Implications and discussion. Pure and Applied Geophysics, 128(3 –4), 501–545. doi: 10.1007/BF00874548.

Coleman R, Lee D, Beatty LB, Brannock WW. 1965. Eclogites and eclogites: Their differences and similarities. Geological Society of America Bulletin, 76(5), 483–508. doi: 10.1130/0016-7606(1965)76[483:EAETDA]2.0.CO.

Dong YL, Wang BD, Zhao WX, Yang TN, Xu JF. 2016. Discovery of eclogite in the Bangong Co-Nujiang ophiolitic mélang, central Tibet,

and tectonic implications. Gondwana Reserch, 35, 115–123. doi: 10.1016/j.gr.2016.03.010.
Dong YS, Li C. 2009. Discovery of eclogite in the Guoganjianian Mountain, central Qiangtang area, northern Tibet, China. Geological Bulletin of China, 28(9), 1197–1200 (in Chinese with English abstract).
Du JX, Zhang LF, Shen XJ, Bader T. 2014. A new *P-T-t* path of eclogites from Chinese southwestern Tianshan: Constraints form *P-T* pseudosections and Sm-Nd isochrom dating. Lithos, 200 –201, 258–272. doi: 10.1016/j.lithos.2014.04.009.
Ernst WG. 2006. Preservation/exhumation of ultrahigh-pressure subduction complexes. Lithos, 92(3–4), 321–335. doi: 10.1016/j.lithos.2006.03.049.
Fan WM, Peng TP, Wang YJ. 2009. Triassic magmatism in the southern Lancangjiang zone, southwestern China and its constraints on the tectonic evolution of Paleo-Tethys. Earth Science Frontiers, 16(6), 291–302 (in Chinese with English abstract).
Fan WM, Wang YJ, Zhang YH, Zhang YZ, Jourdan F, Zi JW, Liu HC. 2015. Paleotethyan subduction process revealed from Triassic blueschists in the Lancang tectonic belt of Southwest China. Tectonophysics, 662, 95–108. doi: 10.1016/j.tecto.2014.12.021.
Genshaft YS, Mironova NA. 1995. Magnetopetrological study of formation conditions of the crustal interior of continents: A case study of kimberlite xenoliths fromYakutia, Siberia. Geomagnetism and Aeronomy, 31, 210–229.
Grimmer JC, Ratschbacher L, Williams M. 2003. When did the ultrahigh-pressure rocks reach the surface? A $^{207}Pb/^{206}Pb$ zircon, $^{40}Ar/^{39}Ar$ while mica, Si-in-white mica, single-grain provenance study of Dabie Shan synorogenic foreland sediments. Chemical Geology, 197(1–4), 87–110. doi: 10.1016/S0009-2541(02)00321-2.
Guillot S, Hattori K, Agard P, Schwartz S, Vidal O. 2009. Exhumation processes in oceanic and continental subduction contexts: A review. In: Lallemand S, Funiciello F, (eds.). Subduction Zone Geodynamics. Berlin-Heidelberg, Springer, 175–205. https://doi.org/10.1007/978–3-540–87974-9_10
Jian P, Liu D, Kröner A, Zhang Q, Wang YZ, Sun XM, Zhang W. 2009. Devonian to Permian plate tectonic cycle of the Paleo-Tethys Orogen in southwest China (II): Insights from zircon ages of ophiolites, arc/back-arc assemblages and within-plate igneous rocks and generation of the Emeishan CFB province. Lithos, 113(3 –4), 767–784. doi: 10.1016/j.lithos.2009.04.006.
Klemd R, Gao J, Li JL, Meyer M. 2015. Metamorphic evolution of (ultra)-high-pressure subduction-related transient crust in the South Tianshan Orogen (Central Asian Orogenic Belt): Geodynamic implications. Gondwana Research, 28(1), 1–25. doi: 10.1016/j.gr.2014.11.008.
Kong HL, Dong GC, Mo XX, Zhao ZD, Zhu DC, Wang S, Li R, Wang QL. 2012. Petrogenesis of Lincang granites in Sanjiang area of western Yunnan Province: Constraints from geochemistry, zircon U-Pb geochronology and Hf isotope. Acta Petrologica Sinica, 28(5), 1438–1452 (in Chinese with English abstract).
Krebs M, Schertl HP, Maresch WV, Draper G. 2011. Mass flow in serpentinite-hosted subduction channels: *P-T-t* path patterns of metamorphic blocks in the Rio San Juan melange (Dominican Republic). Journal of Asian Earth Sciences, 42(4), 569–595. doi: 10.1016/j.jseaes.2011.01.011.
Kusky TM, Bradley DC, Haeussler P, Karl S. 1997. Controls on accretion of flysch and mélange belts at convergent margins: Evidence from the Chugach Bay thrust and Iceworm mélange, Chugach terrane, Alaska. Tectonics, 16(6), 855–878. doi: 10.1029/97TC02780.
Leake BE, Wooley AR, Arps CES, Birch WD, Gilbert MC, Grice JD, Hawthome FC, Kalo A, Kisch HJ, Krivovichev VG, Linthout K, Laird J, Mandarino JA, Maresch WV, Nickel EH, Rock NMS, Schumacher JC, Smith DC, Stephenson NCN, Ungaretti L, Whittaker EJW, Guo YZ. 1997. Nomenclature of amphiboles: Report of the subcommittee on amphiboles of the international mineralogical association commission on new minerals and mineral names. American Mineralogist, 61(405), 295–310. doi: 10.1180/minmag.1997.061.405.13.
Li C, Dong YS, Zhai QG, Wang LQ, Yan QR, Wu YW, He TT. 2008. Discovery of eopaleozoic ophiolite in the Qiangtang of Tibet Plateau: Evidence from SHRIMP U-Pb dating and its tectonic implications. Acta Petrologica Sinica, 24(1), 31–36 (in Chinese with English abstract).
Li C, Wu YW, Wang M, Yang HT. 2010. Significant progress on Pan-African and Early Paleozoic orogenic events in Qinghai-Tibet Plateau-Discovery of Pan-African orogenic unconformity and cambrian system in the Gangdise Area, Tibet, China. Geological Bulletin of China, 29(12), 1733–1736 (in Chinese with English abstract).
Li C, Zhai Q, Dong YS, Liu S, Xie C, Wu Y W. 2009. High-pressure eclogite-blueschist metamorphic belt and closure of Paleo-Tethys Ocean in Central Qiangtang, Qinghai-Tibet Plateau. Journal of Earth Science, 20(2), 209–218. doi: 10.1007/s12583-009-0021-4.
Li J, Sun ZB, Xu GX, Zhou K, Huang L, Tian SM, Zeng WT, Chen GY, Liu GC. 2015. Firstly discovered garnet-amphibolite from Mengku area, Shuangjiang County, Western Yunnan Province, China. Acta Mineralogica Sinica, 35(4), 421–424 (in Chinese with English abstract).
Li J, Sun ZB, Huang L, Xu GX, Tian SM, Deng RH, Zhou K. 2017. *P-T-t* path and geological significance of retrograded eclogites from Mengku area in western Yunnnan Province, China. Acta Petrologica Sinica, 33(7), 2285–2301 (in Chinese with English abstract).
Li JL, Gao J, Wang XS. 2016a. A subduction channel model for exhumation of oceanic-type high-pressure to ultrahigh-pressure eclogite-facies metamorphic rocks in SW Tianshan, China. Science China Earth Sciences, 59(12), 2339–2354. doi: 10.1007/s11430-016-5103-7.
Li JL, Klemd R, Gao J, John T. 2016b. Poly-cyclic metamorphic evolution of eclogite: Evidence for multistage burial-exhumation cycling in a subduction channel. Journal of Petrology, 57(1), 119–146. doi: 10.1093/petrology/egw002.
Li JL, Klemd R, Gao J, Meyer M. 2012. Coexisting carbonate-bearing eclogite and blueschist in SW Tianshan, China: Petrology and phase equilibria. Journal of Asian Earth Sciences, 60, 174–187. doi: 10.1016/j.jseaes.2012.08.015.
Liang X, Wang GH, Yang B, Ran H, Zheng YL, Du JX, Li LG. 2017. Stepwise exhumation of the Triassic Lanling high-pressure metamorphic belt in Central Qiangtang, Tibet: Insights from a coupled study of metamorphism, deformation, and geochronology. Tectonics, 36(4), 652–670. doi: 10.1002/2016TC004455.
Liou JG, Tsujimori T, Zhang RY, Katayama I, Maruyama S. 2004. Global UHP metamorphism and continental subduction/collision: The Himalayan model. International Geology Review, 46(1), 1–27. doi: 10.2747/0020-6814.46.1.1.
Liu GC, Sun ZB, Zeng WT, Feng QL, Huang L, Zhang H. 2017. The age of Wanhe ophiolitic mélange from Mengku area, Shuangjiang County, western Yunnan Province, and its geological significance. Acta Petrologica et Mineralogica, 36(2), 163–174 (in Chinese with English abstract).
Liu Y, Santosh M, Zhao ZB, Niu WC, Wang GH. 2011. Evidence for palaeo-Tethyan oceanic subduction within central Qiangtang, northern Tibet. Lithos, 127(1–2), 39–53. doi: 10.1016/j.lithos.2011.07.023.
Maruyama S, Lou JG, Tarabayashi M. 1996. Blueschists and eclogites of the world and their exhumation. International Geology Review, 38(6), 485–594. doi: 10.1080/00206819709465347.
Metcalfe I. 2011. Palaeozoic-Mesozoic history of SE Asia. Geological Society London Special Publications, 355(1), 7–35. doi: 10.1144/SP355.2.
Morimoto N, Fabries J, Ferguson AK, Ginzburg IV, Ross M, Seifert FA, Zussman J, Aoki K, Gottardi G. 1988. Nomenclature of pyroxenes. American Mineralogist, 73(9–10), 1123–1133. doi: 10.1007/BF01226262.
Nie XM, Feng QL, Qian X, Wang YJ. 2015. Magmatic record of Prototethyan evolution in SW Yunnan, China: Geochemical, zircon U-Pb geochronological and Lu-Hf Isotopic evidence from the Huimin metavolcanics rocks in the Southern Lancangjiang Zone. Gondwana Research, 28(2), 757–768. doi: 10.1016/j.gr.2014.05.011.
Ning WB, Wang JP, Xiao D, Li FF, Huang B, Fu D. 2019. Electron probe microanalysis of monazite and its applications to U-Th-Pb dating of geological samples. Journal of Earth Science, 30(5), 952–963. doi: 10.1007/s12583-019-1020-8.
Peng T, Wang Y, Zhao G, Fan W, Peng B. 2008. Arc-like volcanic rocks from the southern Lancangjiang zone, SW China: Geochronological and geochemical constraints on their petrogenesis and tectonic implications. Lithos, 102(1–2), 358–373. doi: 10.1016/j.lithos.2007.08.012.
Peng TP, Wang YJ, Fan WM, Liu D, Miao L. 2006. SHRIMP zircon U-Pb geochronology of Early Mesozoic felsic igneous rocks from the southern Lancangjiang and its tectonic implications. Science in China (Series D), 36(2), 123–132 (in Chinese with English abstract).
Peng XJ, Luo WL. 1982. The discovery and earth tectonic significance of the blueschist belt in Lancangjiang South Segment of West Yunnan. Regional Geology of China, (2), 69–75 (in Chinese with English abstract).
Peng ZM, Geng QR, Pan GT, Wang LQ, Zhang Z, Cong F, Guan JL. 2014a. Zircon SHRIMP geochronology and Nd-Pb isotopic characteristics of the meta-basalt in the central part of Tibetan Plateau's Qiangtang region. Science China: Earth Sciences, 57, 428–438. doi: 10.1007/s11430-013-4693-3.
Peng ZM, Geng QR, Wang LQ, Zhang Z, Guan JL, Cong F, Liu SS. 2014b. Zircon U-Pb ages and Hf isotopic characteristics of granitic

gneiss from Bunsumco, central Qiangtang, Qinghai-Tibet Plateau. Chinese Science Bulletin, 59(26), 2621–2629 (in Chinese with English abstract). doi: 10.1360/N972014-00014.

Peng ZM, Hu JF, Fu YZ, Zhang J, Guan JL, Han WW, Liu YH, Zhang Z. 2018a. Geological map of Wendong sheet (F47E005016) (1∶50000), the People's Republic of China, In Press.

Peng ZM, Wang GZ, Wang BD, Wang LQ, Fu YZ, Guan JL, Hu JF, Zhang J. 2019. Discovery of glaucophane eclogites within the Lancang Group in Bangbing area, western Yunnan. Journal of Chengdu University of Technology (Science and Technology Edition), 46(5), 639–640 (in Chinese with English abstract).

Peng ZM, Zhang J, Guan JL, Zhang Z, Han WW, Fu YZ. 2018b. The discovery of Early-Middle Ordovician granitic gneiss from the giant Lincang batholith in Sanjiang area of western Yunnan and its geological implications. Earth Science, 43(8), 2571–2585 (in Chinese with English abstract).

Ravna EJK, Terry MP. 2004. Geothermobarometry of UHP and HP eclogites and schists —— an evaluation of equilibria among garnet-clinopyroxene-kyanite-phengite-coesite/quartz. Journal of Metamorphic Geology, 22(6), 579–592. doi: 10.1111/j.1525-1314.2004.00534.x.

Ravna K. 2000. The garnet-clinopyroxene Fe^{2+}-Mg geothermometer: An updated calibration. Journal of Metamorphic Geology, 18(2), 211–220. doi: 10.1046/j.1525-1314.2000.00247.x.

Sone M, Metcalfe I. 2008. Parallel Tethyan sutures in mainland Southeast Asia: New insights for Palaeo-Tethys closure and implications. Comptes Rendus Geoscience, 340(2–3), 166–179. doi: 10.1016/j.crte.2007.09.008.

Sun ZB, Hu SB, Li J, Duan XD, Liu FL, Zhou K, Zhao JT, Li XJ, Bao JF, Wang YX. 2020. Petrology and metamorphism of blueschist in the Damenglong, Jinghong, Southwest Yunnan and its response to Paleotethyan tectonics. Geology in China (in Chinese with English abstract). https://kns.cnki.net/kcms/detail/11.1167.P.20200804.0852.002.html.

Sun ZB, Hu SB, Zhou K, Zhou TQ, Zhao JT, Wang YX, Zhang XP, Zhang SZ, Wang HN, Wang W. 2019. Petrology, mineralogy and metamorphic *P-T* path of eclogites from the Qianmai area, Lancang County, western Yunnan Province. Geological Bulletin of China, 38(7), 1105–1115 (in Chinese with English abstract).

Sun ZB, Li J, Zhou K, Zeng WT, Duan XD, Zhao JT, Xu GX, Fan YH. 2017. Lithogeochemistry characteristics and geological significance of retrograde eclogite in Mengku area, Shuangjiang County, western Yunnan Province, China. Geoscience, 31(4), 746–756 (in Chinese with English abstract).

Tsujimori T, Sisson VB, Liou JG, Harlow GE, Sorensen SS. 2008. Very-low-temperature record of the subduction process: A review of worldwide lawsonite eclogites. Lithos, 92(3 –4), 609–624. doi: 10.1016/j.lithos.2006.03.054.

Wang BD, Wang LQ, Pan GT, Yin FG, Wang DB, Tang Y. 2013. U-Pb zircon dating of Early Paleozoic gabbro from the Nantinghe ophiolite in the Changning-Menglian suture zone and its geological implication. Chinese Science Bulletion, 58(8), 920–930. doi: 10.1007/s11434-012-5481-8.

Wang BD, Wang LQ, Wang DB, Yin FG, He J, Peng ZM, Yan GC. 2018. Tectonic evolution of the Changning-Menglian proto-paleo Tethys Ocean in the Sanjiang Area, South western China. Earth Science, 43(8), 2527–2550. doi: 10.3799/dqkx.2018.160.

Wang DB, Luo L, Tang Y, Yin FG, Wang BD, Wang LQ. 2016. Zircon U-Pb dating and petrogenesis of Early Paleozoic adakites from the Niujingshan ophiolitic mélange in the Changning-Menglian suture zone and its geological implications. Acta Petrologica Sinica, 32(8), 2317–2329 (in Chinese with English abstract).

Wang F, Liu FL, Ji L, Liu LS. 2017. LA-ICP-MS U-Pb dating of detrital zircon from low-grade metamorphic rocks of the Lancang Group in the Lancangjiang Complex and its tectonic implications. Acta Petrologica Sinica, 33(9), 2975–2985 (in Chinese with English abstract).

Wang F, Liu FL, Ji L, Liu PH, Cai J, Tian ZH, Liu LS. 2016. Petrogenesis and metamorphic evolution of blueschist from Xiaoheijiang-Shangyun area in Lancangjiang metamorphic complex. Acta Petrologica et Mineralogica, 35(5), 804–820 (in Chinese with English abstract).

Wang HN, Liu FL, Li J, Sun ZB, Ji L, Tian ZH, Liu LS, Santosh M. 2019. Petrology, geochemistry and *P-T-t* path of lawsonite-bearing retrograded eclogites in the Changning-Menglian orogenic belt, southeast Tibetan Plateau. Journal of Metamorphic Geology, 39(4), 439–478. doi: 10.1111/jmg.12462.

Wang HN, Liu FL, Santosh M, Cai J, Wang F, Ji L. 2020a. Rapid cold slab subduction of the Paleo-Tethys: Insights from lawsonite-bearing blueschist in the Changning-Menglian orogenic belt, southeastern Tibetan Plateau. Gondwana Research, 85, 189–223. doi: 10.1016/j.gr.2020.05.006.

Wang HN, Liu FL, Sun ZB, Ji L, Zhu JJ, Cai J, Zhou K, Li J. 2020b. A new HP-UHP eclogite belt idebtified in the southeastern tibetan plateau: Tracing the extension of the main Paleaeo-Tethys suture Zone. Journal of Petrology, 61(8), 1–45. doi: 10.1093/petrology/egaa073.

Wang J, Li X, Ning W, Kusky T, Wang L, Polat A, Deng H. 2019. Geology of a Neoarchean suture: Evidence from the Zunhua ophiolitic mélange of the Eastern Hebei Province, North China Craton. GSA Bulletin, 131(11–12), 1943–1964. doi: 10.1130/B35138.1.

Wei CJ, Clarke GL. 2011. Calculated phase equilibria for MORB compositions: A reappraisal of the metamorphic evolution of lawsonite eclogite. Journal of Metamorphic Geology, 29(9), 939–952. doi: 10.1111/j.1525-1314.2011.00948.x.

Wei CJ, Li YJ, Yu Y, Zhang JS. 2010. Phase equilibria and metamorphic evolution of glaucophane-bearing UHP eclogites from the Western Dabieshan Terrane, Central China. Journal of Metamorphic Geology, 28(6), 647–666. doi: 10.1111/j.1525-1314.2010.00884.x.

Wei CJ, Tian ZL, Zhang LF. 2013. Modelling of peak mineral assemblages and *P-T* conditions for high-pressure and ultra highpressure eclogites. Chinese Science Bulletin, 58(22), 2159–2164 (in Chinese with English abstract). doi: 10.1360/csb2013-58-22-2159.

Whitney DL, Evans BW. 2010. Abbreviations for names of rock-forming minerals. American Mineralogist, 95(1), 185–187. doi: 10.2138/am.2010.3371.

Xia QX, Zheng YF. 2011. The composition and chemical zoning in garnet from high to ultra high pressure metamorphic rocks. Acta Petrologica Sinina, 27(2), 433–450 (in Chinese with English abstract).

Xing X, Wang Y, Cawood PA, Zhang Y. 2017. Early paleozoic accretionary orogenesis along northern margin of gondwana constrained by high-Mg metaigneous rocks, SW Yunnan. International Journal of Earth Sciences, 106(5), 1469–1486. doi: 10.1007/s00531-015-1282-z.

Zhai MG, Cong BL, Qiao GS. 1990. Sm-Nd and Rb-Sr geochronology of metamorphic rocks from SW Yunnan orogenic zones, China. Acta Petrologica Sinica, 4, 1–11 (in Chinese with English abstract).

Zhai QG, Jahn BM, Zhang RY, Wang J, Su L. 2011a. Triassic subduction of the Paleo-Tethys in northern Tibet, China: Evidence from the geochemical and isotopic characteristics of eclogites and blueschists of the Qiangtang Block. Journal of Asian Earth Sciences, 42(6), 1356–1370. doi: 10.1016/j.jseaes.2011.07.023.

Zhai QG, Zhang RY, Jahn BM, Li C, Song SG, Wang J. 2011b. Triassic eclogites from central Qiangtang, northern Tibet, China: Petrology, geochronology and metamorphic *P-T* path. Lithos, 125(1 –2), 173–189. doi: 10.1016/j.lithos.2011.02.004.

Zhang LF, Lü Z, Zhang GB, Song SG. 2008. The geological characteristics of oceanic-type UHP metamorphic belts and their tectonic implications: Case studies from Southwest Tianshan and North Qaidam in NW China. Chinese Science Bulletin, 53(20), 3120–3130. doi: 10.1007/s11434-008-0386-2.

Zhang RY, Cong BL, Han XL. 1990. Amphiboles of blueschist in west Yunnan region. Scientia Geologica Sinica, 1, 43–53 (in Chinese with English abstract).

Zhang RY, Cong BL, Maruyama S, Liou JG. 1993. Metamorphism and tectonic evolution of the Lancang paired metamorphic belts, south-western China. Journal of Metamorphic Geology, 11(4), 605–619. doi: 10.1111/j.1525-1314.1993.tb00175.x.

Zhang ZB, Li J, Lü GX, Yu H, Wang FZ. 2004. Characteristics of blueschist in Shuangjiang tectonic mélange zone, West Yunnan province. Journal of China University of Geosciences, 15(2), 224–231 (in Chinese with English abstract).

Zhao J. 1993. A study of muscovites from the Lancang metamorphic belt in western Yunnan and its geological significance. Acta Petrologica et Mineralogica, 12(3), 251–260 (in Chinese with English abstract).

Zhao J, Zhong DL, Wang Y. 1994. Metamorphism of Lancang metamorphic belt, the western Yunnan and its relation to deformation. Acta Petrologica Sinica, 10(1), 27–40 (in Chinese with English abstract).

Zheng YF, Zhao ZF, Chen YX. 2013. Continental subduction channel processes: Plate interface interaction during continental collision. Chinese Science Bulletin, 58(35), 4371–4377. doi: 10.1007/s11434-013-6066-x.